EDGE ARTICLE

Check for updates

All publication charges for this article have been paid for by the Royal Society of Chemistry

Solvent attenuation of dispersion interactions quantified in polar and nonpolar media using rigid CH−π balances

Hao Liu, [ID] Harrison M. Scott, Binzhou Lin, Xiaolong Huang, Mark D. Smith [ID] and Ken D. Shimizu [ID] *

Solvent attenuation of dispersion interactions was quantified using a new class of rigid intramolecular CH−π molecular balances. These balances incorporate small, two-carbon CH donors that minimize solvophobic effects and isolate the dispersion component. Folding energies (ΔG_{exp}) were measured across eight solvents: cyclohexane, toluene, chloroform, ethyl acetate, acetone, acetonitrile, DMSO, and methanol. Attenuation values in nonpolar solvents closely matched those reported by Peter Chen using a bimolecular host-guest system. Our use of a molecular balance also enabled study in polar solvents where the attenuation remained similarly high in polar solvents such as DMSO and methanol. The narrow 75 to 80 percent range observed across all solvents demonstrates the consistency of dispersion attenuation and the effectiveness of molecular balances in quantifying weak noncovalent forces while avoiding interference from solvent driven effects. Comparisons between sp^2 and sp^3 CH donors showed similar dispersion contributions, with sp^2 groups exhibiting stronger overall interactions due to greater electrostatic stabilization. As a result, sp^2 CH groups formed stronger interactions in nonpolar solvents, while both CH types showed similar strengths in polar solvents.

Introduction

London dispersion forces (LDFs) are weak attractive interactions, arising from temporary dipoles generated by the correlated electron motion of neighbouring atoms.[1–3] These interactions are present in all atomic systems.[4,5] As a result, LDFs play a crucial role in determining physical properties like melting and boiling points and contribute to molecular stability and reactivity.[6–9] London dispersion forces were among the earliest recognized non-covalent interactions,[10,11] yet there has been renewed interest in dispersion interactions.[1,3,12,13] Recent advances in computational methods provide an accurate estimation of dispersion energies at lower costs, revealing that dispersion interactions are more widespread and impactful than previously appreciated.[14] This has led to a proliferation in experimental systems such as molecular balances, torsion balances, and host–guest systems designed to quantify dispersion interactions in both the gas phase and solution.[3,15–21]

While the importance of dispersion interactions is clear in the gas phase and solid state, their role in solution is more difficult to assess.[15,20,22] Solvent molecules influence both sides of the equilibrium equation, obscuring or compensating for the solute–solute dispersion interactions (Fig. 1). On the left-hand side, solvent molecules form dispersion and other non-covalent interactions with the solute. On the right-hand side, freed solvent molecules can form cohesive solvent–solvent interactions that contribute to solvophobic effects. Recent estimates by Chen and coworkers of this complex solution equilibria have measured the attenuation of dispersion interactions at 60–80% in nonpolar solvents.[15,23] Thus, dispersion interactions in solution are only 20–40% of their strength of the gas phase.

Because the effects of dispersion interactions are greatly attenuated in solution, previous studies have developed strategies to enhance their detectability. One common approach is to use large, polarizable groups such as adamantanes or long alkyl chains to increase the overall interaction energy to measurable levels.[4,15,19,20,22,24] However, this amplification strategy introduces an additional challenge that solvophobic effects also scale with the size of the surfaces, making it difficult to isolate

Department of Chemistry and Biochemistry, University of South Carolina, Columbia, SC 29208, USA. E-mail: shimizu@mailbox.sc.edu
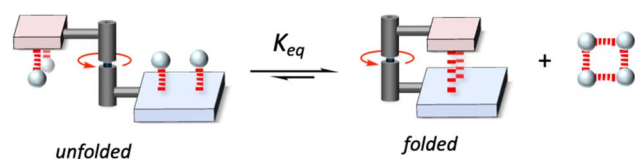
Fig. 1 Representative images of molecular balances designed to measure the dispersion interactions of CH-groups (red rectangles), aromatic surfaces (blue rectangles), and solvents (blue spheres).

the dispersion contribution to the complexation equilibria. In contrast to previous approaches that use large dispersion donors, we introduce a molecular balance system with a small two-carbon unit designed to minimize solvophobic contributions, thereby enabling direct experimental quantification of dispersion attenuation in solution.

Results and discussion

Molecular balance design and synthesis

We designed a series of new molecular balances (**1** and **2**) to study dispersion interactions in solution of CH–π interactions (Fig. 2). CH–π interactions are well-suited for this study because they are dominated by LDFs, owing to the weak polarization of C–H bonds and minimal contributions from electrostatics or hydrogen bonding.[25] Schreiner recently demonstrated that dispersion interactions between alkyl groups as small as ethyl groups could be observed and measured in solution.[19] Building on this observation, we reasoned that the limited surface area of small dispersion donors would produce minimal solvophobic interference, thereby allowing clearer isolation of dispersion contributions. Our balances incorporate small, two-carbon CH and CH$_2$ groups that form intramolecular interactions with various aromatic surfaces, enabling us to probe weak non-covalent forces while minimizing solvophobic effects.

An additional advantage of our intramolecular balance system is its ability to operate in a broader range of solvents than previous bimolecular systems. In Chen's studies of dispersion attenuation, the host–guest complexes relied on hydrogen bonding to maintain the dispersion interaction, limiting measurements to nonpolar solvents that do not disrupt these interactions. In contrast, our balances use a rigid covalent framework to fix the geometry of the interacting groups without relying on hydrogen bonds or other supporting interactions. This allows measurements of CH–π dispersion interactions in both polar and nonpolar solvents, including those with strong hydrogen-bonding disrupting abilities such as THF, DMSO, and methanol. As a result, our system enables a more comprehensive evaluation of dispersion attenuation by extending measurements across a wider and more chemically diverse range of solvents.

The combination of structural rigidity and solvent compatibility in our system allows us to test three key questions: (1) can the magnitude of dispersion attenuation by organic solvents reported by Chen (∼70%) be confirmed using a fundamentally different system and method; (2) does the attenuation persist in polar solvents that disrupt hydrogen bonding and were inaccessible to previous bimolecular systems; and (3) do sp^2 and sp^3 C–H groups form dispersion interactions of different strength?

To enforce a favorable geometry between the dispersion donor and aromatic surface, we employed a rigid yet conformationally dynamic *N*-phenylsuccinimide scaffold. We and others have previously used *N*-arylimide molecular balances to successfully study a variety of weak non-covalent interactions, including aromatic stacking,[26] CH–π,[27] halogen–π,[28] chalcogen–π,[29] substituent–π,[30] and solvent effects.[31] In our balances, rotation about the C$_{(aryl)}$–N$_{(imide)}$ bond gives rise to two interconverting conformers: a folded form, where the CH donor is positioned above the aromatic acceptor, and an unfolded form, where this contact is disrupted (Fig. 2). A unique feature of our design is that both ends of the CH donor are tethered to the framework, more rigidly positioning it over the π-surface. This enhanced geometric control is particularly important for measuring weak interactions. It reduces conformational flexibility and entropic contributions compared to previous dispersion balances, where the donor group was tethered by a single linkage.[19,20,22,31,32]

Our balances also allow systematic variation of two structural features that modulate the intramolecular interaction strength: the hybridization of the CH donor (sp^2 in balance **1** *versus* sp^3 in balance **2**) and the size and orientation of the aromatic π-surface.[33] The π-surface was varied across a series of increasingly polarizable aryl groups. These included phenyl (Ph), 1-naphthyl (Nap), 2-naphthyl (2Nap), 9-anthracenyl (Anth), 1-pyrenyl (Py), and 4-pyrenyl (4Py). If dispersion dominates the CH–π interaction, we expect a systematic increase in folding energy with aryl size. Because the size of the CH donors remains constant, the solvophobic interactions should plateau once the π-surface is large enough to make full contact. This approach complements our previous study, where the aromatic surface was fixed and the size of the alkyl CH donor was varied to probe dispersion.[34] By reversing that design, we achieve greater control over solvent-accessible surface area, enabling clearer separation of dispersion and solvophobic effects.

Balances **1** and **2** were efficiently synthesized in 2 or 3 steps, as shown in Fig. 3. The requisite 2-aryl-5-fluoroanilines were prepared by Suzuki coupling of 2-bromo-5-fluoroaniline with various arylboronic acids.[34] The anilines were thermally condensed with *cis*-5-norbornene-*endo*-2,3-dicarboxylic anhydride to form the atropisomeric *N*-arylimides of balance **1** with
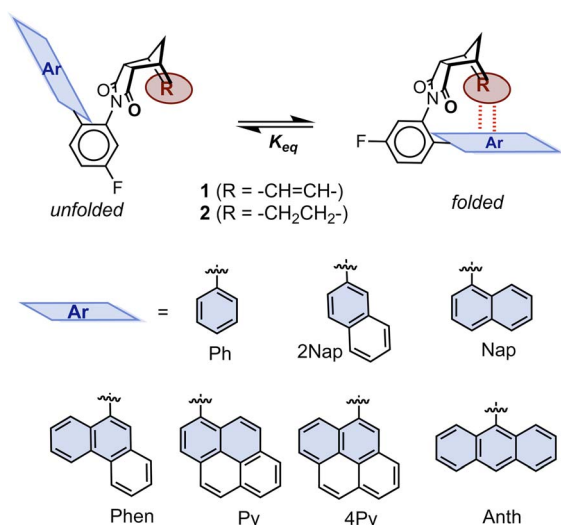

Fig. 2 Schematic representation of the equilibrium for sp^2 and sp^3 molecular balances **1** and **2** with two-carbon vinyl and alkyl dispersion donors which form an intramolecular CH–π interactions. The first row of rings in the aromatic surfaces that can form direct interactions with the CH-groups are highlighted in blue.
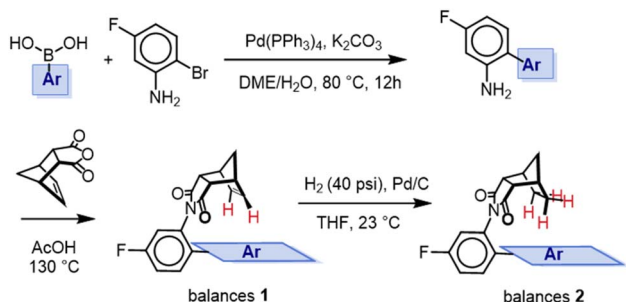
Fig. 3 General synthetic route for molecular balances **1** and **2**.

vinyl CH-groups. The vinyl groups were converted into the alkyl CH-groups of balance **2** *via* hydrogenation. All steps of the synthesis proceeded in yields greater than 70%, even with larger aromatic groups, demonstrating the robustness and versatility of the synthetic route.

Verification and measurement of interaction energies

The ability of the rigid bicyclic framework to position the two carbon units at the appropriate distances and geometry with the aromatic surfaces to form intramolecular CH–π interactions was initially confirmed *via* X-ray crystallographic analysis. The preference for the folded conformers in the solid state was the first indication of the formation of stabilizing dispersion interactions. Balances **1**(Nap), **1**(Phen), **1**(Anth), **1**(2Nap), **1**(4Py), and **2**(4Py) all crystallized in the folded conformation (Fig. 4). Only balance **1**(Py) crystallized in the unfolded conformation, which may be due to the strong intermolecular pyrene–pyrene interactions in the solid state (see SI). In the folded crystal structures, the hydrogens of the alkyl and vinyl groups were positioned over the aromatic shelves within the cutoff distance for CH–π interactions (<3.05 Å).[35] The measured hydrogen-to-plane distances ranged from 2.51 Å to 2.89 Å, consistent with previously reported CH–π interaction distances in crystal structure database surveys (2.35 Å–3.05 Å).[36–38] Notably, contact occurs primarily between the CH groups and the first row of
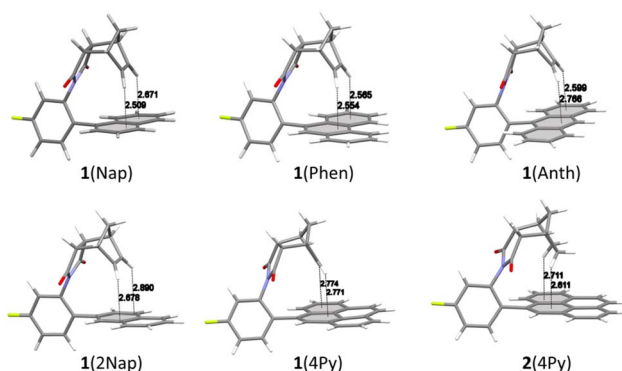

Fig. 4 Side views of the X-ray crystal structures of molecular balances **1** and **2**. The hydrogen-to-plane distance between the CH groups and aromatic shelf is shown in units of angstroms. The rings in the first row of aromatic shelves that form CH–π interactions are highlighted in gray.

aromatic rings, which are highlighted in gray in Fig. 4. In all the folded structures, the distances between CH groups and the first row of aromatic rings were less than 3.05 Å, whereas the corresponding distances to the second row of aromatic rings exceeded this VDW threshold. For example, both aromatic rings of **1**(Nap) can engage in stabilizing dispersion interactions with the CH groups. In contrast, only one aromatic ring in **1**(2Nap) is positioned to interact favourably with the CH groups.

The folding ratios of molecular balances **1** and **2** were initially measured in chloroform *via* integration of the ^{19}F NMR spectra. At room temperature (23 °C), the conformers were in slow exchange, displaying separate sets of peaks for the folded and unfolded conformers. Balance **1**(Ph), featuring the smallest aromatic surface, formed the weakest vinyl-π interaction and served as the control for vinyl CH balances with larger aromatic surfaces (Fig. 5a). Similarly, balance **2**(Ph) formed the weakest alkyl-π interaction and served as the control for the alkyl CH balances (Fig. 5a). These normalized interaction energies ($-\Delta\Delta G_{CDCl_3}$) varied from 0.0 for **1**(Ph) to 1.02 kcal mol^{-1} for **1**(Anth) in CDCl$_3$, depending on the aromatic surface (Fig. 5a).

The strength of the interaction correlated with the number of first row rings in the aromatic surfaces for the vinyl balances **1**. Balances **1**(Ph) and **1**(2Nap), containing only a single aromatic ring accessible to the CHs, exhibited the weakest interactions (0 to 0.**1** kcal mol^{-1} in CDCl$_3$). Balances such as **1**(Py), **1**(Nap), **1**(Phen), and **1**(4Py), which featured two first-row aromatic rings, displayed stronger CH–π interactions (0.41 to 0.92 kcal mol^{-1}). Extending the first-row to three rings for anthracene **1**(Anth) provided further stabilization (1.02 kcal mol^{-1}). These interaction energy trends in CDCl$_3$ are consistent with the number of rings in contact with the CH groups in the folded crystal structures. Notably, the addition of the second row of rings did not lead to further increases in interaction strength. For example, **1**(Nap, 0.81 kcal mol^{-1}), **1**(Phen, 0.89 kcal mol^{-1}), and **1**(4Py, 0.87 kcal mol^{-1}) have two first row rings but varying numbers of second row ring. Yet, all of their interaction energies are very similar. Interestingly, **1**(Py) has a smaller interaction energy than **1**(4Py) even though they exhibit 2 rings in the first row. This is possibly due to additional repulsive interactions in **1**(Py).

The dispersion interactions involving the sp^3 CHs of balances **2** followed similar trends to those of the sp^2 CHs of balances **1** in CDCl$_3$ (Fig. 5a) and DMSO-d$_6$ (Fig. 5b). In CDCl$_3$, the sp^2 CH interactions consistently exhibited 20–40% stronger stabilization in CDCl$_3$. For instance, in balance **1**(Py), the sp^2 CH group showed an interaction energy of 0.45 kcal mol^{-1}, whereas the corresponding sp^3 CH balance (**2**(Py)) exhibited a weaker interaction of 0.18 kcal mol^{-1}. These results are consistent with a stronger electrostatic component due to the greater electrostatic polarization of sp^2 C–H enhancing CH–π dispersion interactions, in agreement with prior computational studies from Tsuzuki.[40] Further support for this electrostatic hypothesis comes from the similar interaction energies of the sp^2 and sp^3 balances **1** and **2** in DMSO-d$_6$ (Fig. 5b). The differences observed in CDCl$_3$ largely disappear in DMSO, consistent with the polar solvent screening or attenuating the electrostatic component. In DMSO, the $-\Delta\Delta G_{DMSO}$ appear to reflect primarily dispersion
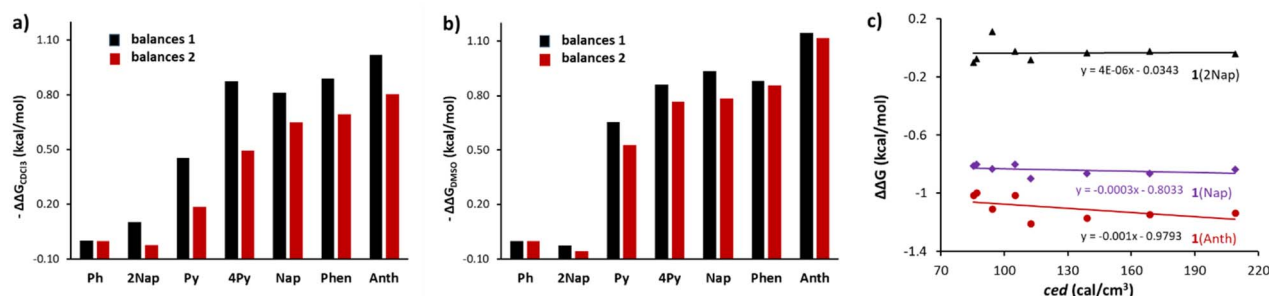
Fig. 5 (a) Normalized NMR-measured folding energies ($-\Delta\Delta G_{CDCl_3}$) of CH double bond (black bar) and sp^3 CH (red bar) with different aromatic shelves in CDCl$_3$. (b) Normalized NMR-measured folding energies ($-\Delta\Delta G_{DMSO}$) of CH double bond (black bar) and sp^3 CH (red bar) with different aromatic shelves in DMSO. The error in the measured folding energy was less than ± 0.02 kcal mol^{-1}.[39] The folding energies of balances **1** and **2** were normalized to **1**(Ph) and **2**(Ph), respectively. (c) Correlation between solvent ced and the normalized NMR-measured folding energies ($\Delta\Delta G$) of balances **1**(2Nap), **1**(Nap), and **1**(Anth) in eight organic solvents.

and solvophobic interactions, which are very similar for both CH types. Comparison of the folding free energies in CDCl$_3$ and DMSO-d_6 thus provides insight into the relative contributions of electrostatic and dispersion effects. The dominant role of dispersion in the CH–π interaction[25] is evident from the similar $\Delta\Delta G$ values measured in DMSO-d_6 and CDCl$_3$. Because DMSO is highly polar and effectively screens electrostatic interactions, the comparable folding energies in both solvents suggest that dispersion, which is not strongly affected by solvent polarity, is the primary contributor.

Assessing the solvophobic effect

Further solvent studies were conducted to determine whether the observed folding trends had a significant solvophobic component. The folding free energies of balances **1** and **2** were measured in eight organic solvents. Monitoring the fluorine NMR-tag *via* ^{19}F NMR enabled the use of both deuterated and non-deuterated solvents, including CDCl$_3$, THF, acetone, 1,4-dioxane, pyridine, DMF, DMSO-d_6, and methanol (Fig. 5c). These solvents have cohesive energy densities (ced) ranging from 85.4 (CDCl$_3$) to 209 (MeOH), which serves as a useful predictor of the strength of solvophobic interactions. Previously, Cockroft and our study showed a positive linear correlation between solvent ced and the solvophobic effect, as higher ced solvents had proportionally stronger solvophobic effects.[31,32] This correlation is attributed to the ability of the solvent parameter ced to assess the strength of the solvent–solvent interactions on the right-hand side of folding equilibrium (Fig. 1), which is a major component of the solvophobic effect. The $\Delta\Delta G$ values for balances **1** and **2** stayed constant with increasing the solvent ced values, suggesting a minimal solvophobic contribution to the folding behaviour of these systems (Fig. 5c).

The origins of the minimal solvophobic effects in **1** and **2** were examined. The solvent-accessible surface area (SASA) values for the folded and unfolded conformers of balances **1** and **2** were calculated using Spartan 24, based on geometries derived from their corresponding crystal structures (see SI). The change in the SASA (ΔSASA) upon folding was very small, <6 Å^2 for all balances, due to the small size of the CH dispersion

donors. We used these values to calculate the expected solvophobic effects in chloroform and DMSO from the ΔSASA and ced values using our recently developed empirical model.[31] The solvophobic interactions were all <0.05 kcal mol^{-1}, which is consistent with the observed negligible solvophobic effects. For example, for balances **1**(Anth) and **2**(Anth), the solvophobic interactions in CDCl$_3$ and DMSO in this study are −0.02 and −0.04 kcal mol^{-1}.

The minimal solvophobic effects provided a unique opportunity to directly assess the magnitude of solvent attenuation on dispersion interactions and to test recent estimates of 70% attenuation by Chen.[15] To provide an estimate of the gas phase dispersion interaction strengths, the computational methods validated by Chen were employed. Interaction energies were calculated for balances **1** and **2** using density functional theory (DFT). First, both folded and unfolded structures were optimized using the B97-D3 functional with the aug-cc-pVDZ basis set. Then, single-point energy calculations were performed on these optimized structures using the M06-L functional with the def2-QZVP basis set. A plot of the experimental (ΔG) *versus* calculated (ΔG_{cal}) folding energies (Fig. 6) provided support for the accuracy of the DFT calculations. A strong linear correlation was observed with an R^2 of 0.9. Furthermore, the sp^2 and sp^3 balances **1** and **2** follow the same line providing additional support for the accuracy of the DFT calculations.

To assess the solvent attenuation of the dispersion, the slope of the experimental *versus* calculated folding energies plot was examined (Fig. 6a). The slope of 0.22 indicated that dispersion interactions in the gas phase are approximately four times stronger than in chloroform, which corresponds to a 78% ± 2% reduction in interaction strength. A similar analysis of the slope in other organic solvents, including THF (0.20), acetone (0.24), pyridine (0.24), DMF (0.25), DMSO (0.24), MeOH (0.23), and 1,4-dioxane (0.21), gave attenuation values of 75–80% (see SI). These values are remarkably similar to Chen's study estimates of 60–80% attenuation in polar and nonpolar aprotic solvents, which were obtained using a different methodology and a bimolecular complexation model system.[15,23] Despite an average attenuation of ~77% in organic solvents, dispersion interactions remain an impactful stabilizing force. These
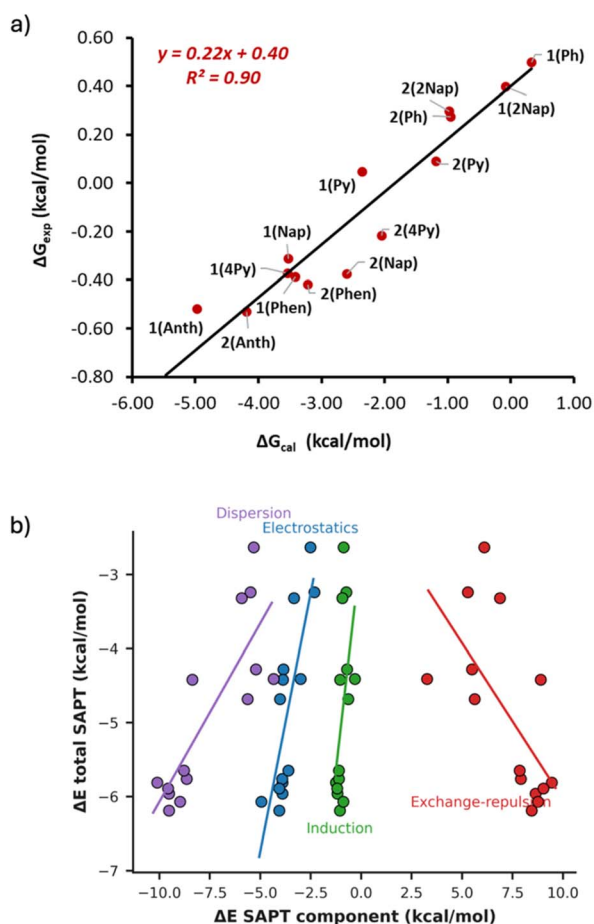
Fig. 6 (a) Plots of the experimental folding energies in CDCl$_3$ of **1** and **2** *versus* the DFT calculated folding free energies (M06-L/def2-QZVP// B97-D3/aug-cc-PVDZ). (b) Correlation between difference in the total SAPT interaction energies for the folded and unfolded conformers of **1** and **2** and the individual differences in SAPT components (exchange-repulsion ΔE_{exch}, electrostatics ΔE_{elst}, induction ΔE_{ind}, and dispersion ΔE_{disp}) calculated for the folded geometries of the molecular balances at the SAPT0/jun-cc-pVDZ level using the functional group interaction analysis method (Fi-SAPT) in Psi4. The π surfaces, norbornene, and the remaining framework were treated as separate fragments in the energy decomposition analysis.

findings underscore the critical role of dispersion forces in molecular stability and highlight their potential as a guiding principle in the design of chemically stable systems. This agreement supports the reliability of the attenuation effect and highlights the value of using distinct, independent strategies to quantify weak noncovalent interactions in solution.

To further investigate the origin of the stabilization observed for the folded conformers and to quantify the contributions of different noncovalent forces, we performed symmetry-adapted perturbation theory (SAPT) calculations on the folded and unfolded geometries (Fig. 6b). This analysis was carried out at the SAPT0/jun-cc-pVDZ level using the functional group interaction analysis (Fi-SAPT) method in Psi4. The molecular balances were partitioned into three fragments: the π surface, the norbornene, and the remaining framework, which allowed isolation of the donor–acceptor interaction between the CH donors and

the π surface. The folded–unfolded energy differences (ΔE_{total}) were decomposed into exchange-repulsion (ΔE_{exch}), electrostatics (ΔE_{elst}), induction (ΔE_{ind}), and dispersion (ΔE_{disp}) components. The results show that the dispersion term is the dominant attractive interaction, confirming that folding promotes strong dispersion contacts between the aromatic surfaces. The magnitude of the exchange-repulsion term correlates with that of the attractive components, indicating a compensating increase in repulsion as the attractive interactions strengthen. Dispersion is significantly greater in magnitude than the electrostatic and induction terms, supporting the conclusion that dispersion forces are the primary stabilizing factor in the folded conformations of these molecular balances.

The narrow range of attenuation values (75–80%) observed across solvents with very different cohesive energy densities provides strong evidence that our system effectively isolates the dispersion component. This uniformity arises because solvophobic contributions have been minimized. If solvophobic effects were significant, ΔG_{exp} would vary more strongly with solvent due to differences in solvent cohesion. Moreover, the consistent attenuation across solvents is consistent with expectations, as most nonfluorinated organic solvents have similar polarizabilities and therefore form solvent–solvent and solvent–solute dispersion interactions of comparable strength.

Conclusions

In conclusion, a series of *N*-phenylimide molecular balances was developed to investigate weak London dispersion forces of CH–π interactions in organic solvents. These balances restrict rotation around the central C$_{(phenyl)}$–N$_{(imide)}$ bond, adopting distinct folded and unfolded conformers that enable quantification of interaction energies through ^{19}F NMR-measured equilibria in eight solvents with varying *ced*. The dispersion interactions were first observed by the preference of the folded crystal conformer for balances **1**(Nap), **1**(Phen), **1**(Anth), **1**(2Nap), **1**(4Py), and **2**(4Py). Then, the ΔG values in the solution phase showed that the strength of the interaction positively correlated with the number of first row rings in the aromatic surfaces for both balances **1** and **2**, which can form direct contact with the CH-groups. Comparisons between sp^3 (CH$_2$– CH$_2$) and sp^2 (CH=CH) units reveal similar trends, with sp^2 groups exhibiting stronger interactions in chloroform but similar interactions in DMSO. This is consistent with the sp^2 CH–π interactions having stronger electrostatic components but similar dispersion components as sp^3 CH–π interactions. The use of small two-carbon CH donors minimized solvophobic effects, enabling isolation of the dispersion component of the interaction. The ΔG_{exp} measured in eight organic solvents correlated strongly with computed gas phase interaction energies and revealed a consistent 75 to 80 percent attenuation of dispersion strength. These values closely matched those reported by Chen[15] in nonpolar solvents and extended them to polar solvents such as DMSO and methanol, which were inaccessible in previous systems due to hydrogen bond disruption. The narrow range of attenuation across all solvents demonstrates that dispersion attenuation is relatively insensitive to

solvent polarity and highlights the reliability of the balance system in isolating weak noncovalent interactions. Despite this dramatic attenuation, dispersion interactions remain a significant stabilizing force in organic solvents. These findings underscore the critical role of dispersion forces in molecular stability and highlight their potential as a guiding principle for designing and optimizing chemical processes.

Experimental

Synthesis of balances 1 and 2

Fig. 3 depicts the general synthetic approach for the synthesis of molecular balances **1** and **2** in this study. The general reaction procedures are as follows.

The 2-aryl-5-fluoroanilines were synthesized using Suzuki coupling conditions.[34] A dry pressure tube flushed with nitrogen and equipped with a magnetic stirrer bar was charged with arylboronic acid (1.5 equiv.), K_2CO_3 (4.0 equiv), and $Pd(PPh_3)_4$ (10 mol%). A 0.25 M solution of 2-bromo-5-fluoroaniline in DME/H_2O (1:1) was added, and the resulting mixture was heated to 80 °C for 12 hours. The reaction mixture was then poured into water and extracted with CH_2Cl_2 (3–5 times), dried over anhydrous Na_2SO_4, and concentrated under reduced pressure. The residue was purified by column chromatography on silica gel to give the corresponding 2-aminoaryl product.

Synthesis of balances 1

The reactants, *cis*-5-norbornene-*endo*-2,3-dicarboxylic anhydride (1 mmol) and 2-aryl-5-fluoroanilines (1 mmol), and 3 mL AcOH were added to a pressure tube. The tube was sealed and heated to 110 °C for 24 hours. After cooling to room temperature, the reaction mixture was poured into 50 mL of water and extracted three times with 30 mL portions of ethyl acetate. The combined organic layers were separated and the solvent removed under reduced pressure. The pure product was obtained by recrystallization from EtOAc/hexane as a yellow solid.

Synthesis of balances 2

Balance **1** (0.30 mmol) was dissolved in 10 mL of THF, and palladium on carbon catalyst (0.03 mmol) was added to the solution. The solution was reacted with hydrogen gas (40 psi) for 4 h in a Parr shaker, after which the palladium on the carbon catalyst was removed by filtering through Celite, and the THF was removed under reduced pressure. After recrystallization from EtOAc and hexane, balance **2** were obtained.

Measurement of the folding free energies

The folded/unfolded ratios were measured by integration of the ^{19}F NMR spectra at 25 °C. The peak areas of the singlets corresponding to the folded/unfolded ratios were measured by line fitting analysis. The folding free energies were calculated from the equation $\Delta G_{exp} = -RT \ln([folded]/[unfolded])$. The error in ΔG_{exp} was estimated to be ± 0.02 kcal mol^{-1} based on a conservative estimate of the NMR measured folded/unfolded ratio of 3%.[39]

Computational details

The optimized folded and unfolded structures for balances **1** and **2** were calculated (M06-L/def2-QZVP//B97-D3/aug-cc-PVDZ) in Spartan24. Convergence criteria were 10^{-4} hartree/bohr for the maximum Cartesian gradient and 10^{-4} angstrom for the maximum atomic displacement. Geometry optimizations were performed using the B97-D3 method, which was consistent with the approach used by Chen,[15] while the M06-L functional was employed to compute the folding energies (ΔE and ΔG) of all molecular balances. The solvent-accessible surface areas (SASA) of the folded and unfolded conformers of the balances were calculated using density functional theory (DFT) at the B97-D3/aug-cc-PVDZ level of theory with a 1 Å probe in Spartan 24. ΔSASA (Å^2) was measured by subtracting the folded conformer SASA from the unfolded conformer SASA.

Author contributions

H. L. designed the experiments, performed the data analysis, and wrote the original draft of the manuscript; H. S., B. L. and X. H. carried out the synthesis, performed the data analysis and theoretical analysis; M. S. performed X-ray crystallography and data analysis; K. S. supervised the project and revised the manuscript; all authors discussed the data. All authors reviewed and edited the manuscript.

Conflicts of interest

The authors declare no competing financial interests.

Data availability

CCDC 2442964–2442966, 2442968, 2442969, 2442971 and 2442973 contain the supplementary crystallographic data for this paper.[41a–g]

Supplementary information: Experimental details; X-ray and $^1H/^{13}C$ NMR data; details of data analyses and solvent studies. CCDC 2442964, 2442965, 2442966, 2442968, 2442969, 2442971, 2442973. See DOI: https://doi.org/10.1039/d5sc02852c.

Acknowledgements

This work was supported by the National Science Foundation Grants CHE 2304777.

Notes and references

1 J. P. Wagner and P. R. Schreiner, *Angew. Chem., Int. Ed.*, 2015, **54**, 12274–12296.
2 H.-J. Schneider, *Acc. Chem. Res.*, 2015, **48**, 1815–1822.
3 L. Rummel and P. R. Schreiner, *Angew. Chem., Int. Ed.*, 2024, **63**, e202316364.
4 L.-A. Gravillier and S. L. Cockroft, *Acc. Chem. Res.*, 2023, **56**, 3535–3544.
5 H. Liu and K. D. Shimizu, *Acc. Chem. Res.*, 2023, **56**, 3572–3580.

6 H. Aikawa, Y. Takahira and M. Yamaguchi, *Chem. Commun.*, 2011, **47**, 1479–1481.

7 J. Gramüller, M. Franta and R. M. Gschwind, *J. Am. Chem. Soc.*, 2022, **144**, 19861–19871.

8 T. H. Webb and C. S. Wilcox, *Chem. Soc. Rev.*, 1993, **22**, 383–395.

9 J. S. S. K. Formen, J. R. Howard, E. V. Anslyn and C. Wolf, *Angew. Chem., Int. Ed.*, 2024, **63**, e202400767.

10 F. London, *Trans. Faraday Soc.*, 1937, **33**, 8b–26.

11 F. London, *Z. Phys.*, 1930, **63**, 245–279.

12 D. J. Liptrot and P. P. Power, *Nat. Rev. Chem.*, 2017, **1**, 1–12.

13 M. Bursch, E. Caldeweyher, A. Hansen, H. Neugebauer, S. Ehlert and S. Grimme, *Acc. Chem. Res.*, 2019, **52**, 258–266.

14 S. Grimme, *WIRES Comput. Mol. Sci.*, 2011, **1**, 211–228.

15 R. Pollice, M. Bot, I. J. Kobylianskii, I. Shenderovich and P. Chen, *J. Am. Chem. Soc.*, 2017, **139**, 13126–13140.

16 J. Hwang, B. E. Dial, P. Li, M. E. Kozik, M. D. Smith and K. D. Shimizu, *Chem. Sci.*, 2015, **6**, 4358–4364.

17 K. I. Assaf and W. M. Nau, *Acc. Chem. Res.*, 2023, **56**, 3451–3461.

18 L. Yang, J. B. Brazier, T. A. Hubbard, D. M. Rogers and S. L. Cockroft, *Angew. Chem., Int. Ed.*, 2016, **55**, 912–916.

19 F. M. Wilming, B. Marazzi, P. P. Debes, J. Becker and P. R. Schreiner, *J. Org. Chem.*, 2023, **88**, 1024–1035.

20 A. Elmi, K. M. Bąk and S. L. Cockroft, *Angew. Chem., Int. Ed.*, 2024, **63**, e202412056.

21 L. Yang, C. Adam, G. S. Nichol and S. L. Cockroft, *Nat. Chem.*, 2013, **5**, 1006–1010.

22 M. A. Strauss and H. A. Wegner, *Angew. Chem., Int. Ed.*, 2021, **60**, 779–786.

23 R. Pollice, F. Fleckenstein, I. Shenderovich and P. Chen, *Angew. Chem., Int. Ed.*, 2019, **58**, 14281–14288.

24 C. Adam, L. Yang and S. L. Cockroft, *Angew. Chem., Int. Ed.*, 2015, **54**, 1164–1167.

25 S. Tsuzuki and A. Fujii, *Phys. Chem. Chem. Phys.*, 2008, **10**, 2584–2594.

26 W. R. Carroll, P. Pellechia and K. D. Shimizu, *Org. Lett.*, 2008, **10**, 3547–3550.

27 W. R. Carroll, C. Zhao, M. D. Smith, P. J. Pellechia and K. D. Shimizu, *Org. Lett.*, 2011, **13**, 4320–4323.

28 P. Li, J. M. Maier, E. C. Vik, C. J. Yehl, B. E. Dial, A. E. Rickher, M. D. Smith, P. J. Pellechia and K. D. Shimizu, *Angew. Chem., Int. Ed.*, 2017, **56**, 7209–7212.

29 J. Hwang, P. Li, M. D. Smith, C. E. Warden, D. A. Sirianni, E. C. Vik, J. M. Maier, C. J. Yehl, C. D. Sherrill and K. D. Shimizu, *J. Am. Chem. Soc.*, 2018, **140**, 13301–13307.

30 J. Hwang, P. Li, W. R. Carroll, M. D. Smith, P. J. Pellechia and K. D. Shimizu, *J. Am. Chem. Soc.*, 2014, **136**, 14060–14067.

31 A. N. Manzewitsch, H. Liu, B. Lin, P. Li, P. J. Pellechia and K. D. Shimizu, *Angew. Chem., Int. Ed.*, 2024, **63**, e202314962.

32 L. Yang, C. Adam and S. L. Cockroft, *J. Am. Chem. Soc.*, 2015, **137**, 10084–10087.

33 C. Zhao, P. Li, M. D. Smith, P. J. Pellechia and K. D. Shimizu, *Org. Lett.*, 2014, **16**, 3520–3523.

34 T. Yuan, K. Fu and L. Shi, *Org. Chem. Front.*, 2024, **11**, 4529–4538.

35 M. Nishio, Y. Umezawa, K. Honda, S. Tsuboyama and H. Suezawa, *CrystEngComm*, 2009, **11**, 1757–1788.

36 H. Takahashi, S. Tsuboyama, Y. Umezawa, K. Honda and M. Nishio, *Tetrahedron*, 2000, **56**, 6185–6191.

37 M. Nishio, *Phys. Chem. Chem. Phys.*, 2011, **13**, 13873.

38 Y. Umezawa, S. Tsuboyama, H. Takahashi, J. Uzawa and M. Nishio, *Bioorg. Med. Chem.*, 1999, **7**, 2021–2026.

39 P. Li, E. C. Vik and K. D. Shimizu, *Acc. Chem. Res.*, 2020, **53**, 2705–2714.

40 S. Tsuzuki, K. Honda, T. Uchimaru, M. Mikami and K. Tanabe, *J. Am. Chem. Soc.*, 2000, **122**, 3746–3753.

41 (*a*) H. Liu, H. M. Scott, B. Lin, X. Huang, M. D. Smith and K. D. Shimizu, CCDC 2442964: Experimental Crystal Structure Determination, 2025, DOI: **10.5517/ccdc.csd.cc2n0393.**; (*b*) H. Liu, H. M. Scott, B. Lin, X. Huang, M. D. Smith and K. D. Shimizu, CCDC 2442965: Experimental Crystal Structure Determination, 2025, DOI: **10.5517/ccdc.csd.cc2n03b4**; (*c*) H. Liu, H. M. Scott, B. Lin, X. Huang, M. D. Smith and K. D. Shimizu, CCDC 2442966: Experimental Crystal Structure Determination, 2025, DOI: **10.5517/ccdc.csd.cc2n03c5**; (*d*) H. Liu, H. M. Scott, B. Lin, X. Huang, M. D. Smith and K. D. Shimizu, CCDC 2442968: Experimental Crystal Structure Determination, 2025, DOI: **10.5517/ccdc.csd.cc2n03f7**; (*e*) H. Liu, H. M. Scott, B. Lin, X. Huang, M. D. Smith and K. D. Shimizu, CCDC 2442969: Experimental Crystal Structure Determination, 2025, DOI: **10.5517/ccdc.csd.cc2n03g8**; (*f*) H. Liu, H. M. Scott, B. Lin, X. Huang, M. D. Smith and K. D. Shimizu, CCDC 2442971: Experimental Crystal Structure Determination, 2025, DOI: **10.5517/ccdc.csd.cc2n03jb**; (*g*) H. Liu, H. M. Scott, B. Lin, X. Huang, M. D. Smith and K. D. Shimizu, CCDC 2442973: Experimental Crystal Structure Determination, 2025, DOI: **10.5517/ccdc.csd.cc2n03ld**.